Rotating Stratified Flow over Finite Isolated Topography

LEE-OR MERKINE AND EUGENIA KÁLNAY-RIVAS

Department of Meteorology, Massachusetts Institute of Technology, Cambridge 02139

(Manuscript received 18 September 1975, in revised form 9 February 1976)

ABSTRACT

Inviscid, steady, stratified rotating flow over a finite, isolated topographic feature is critically analyzed. The formulation is based on approximating the horizontal momentum by the geostrophic momentum. A boundary value problem governs the perturbation pressure field. The solution is an anticyclonic, topographically-bound vortex whose characteristics are independent of the upstream velocity but do depend on stratification, rotation, and the nature of the topography. The vortex is baroclinic in the vicinity of the mountain but barotropic in the far field. The velocity field is a combination of the bound vortex and an upstream velocity interacting with the perturbation pressure field. The effects of stratification, upstream velocity and the nature of the topography are investigated, and fluid trajectories are plotted.

1. Introduction

The need for deep understanding of flow response to topographic forcing is of unquestionable importance both in meteorology and oceanography, even more so when the horizontal dimensions of the topography are such that rotation influences the dynamics of the flow. An important example is the problem of topographically induced cyclogenesis.

It is well known in meteorology that the lee side of mountain ridges is a favorable site for cyclogenesis (Petterssen, 1956). Notable examples are the vast Rockies and the much more compact Alps. This phenomenon has also been demonstrated in numerical experiments using large-scale general circulation models (Manabe and Terpstra, 1974; Egger, 1972), which however failed to explain its physics. The failure can be attributed to the insufficient diagnosis which is augmented by poor resolution of the topography.

Recently two attempts have been made to probe into the mechanism of topographically induced cyclogenesis. Merkine (1975) considered the interaction of vertically sheared, inviscid steady flow with an infinitely long ridge and concluded that baroclinic instability may be initiated on the lee side of the ridge. Huppert and Bryan (1975) solved numerically an initial value problem using the primitive equations with cyclic boundary conditions. They demonstrated that during the transient stage and under certain conditions a cyclonic vortex may be shed from the topography. This process may be another possible mechanism for cyclogenesis.

Other recent investigations of flow-topography interactions were mainly concerned with the conditions necessary for the initiation of inertial Taylor columns (Ingersoll, 1969; Hogg, 1973; Huppert, 1975; McCartney, 1975). All these studies are based on the quasi-geostrophic approximation.

In spite of the numerous studies of the mountain problem we still have not built a sufficient degree of understanding of the physical processes involved. Lack of experimental and observational evidence is, of course, another major obstacle in improving our understanding. Furthermore, it is the authors' opinion that even the available theoretical models have not been exploited to the fullest extent.

The purpose of this work is to analyze more carefully the details of the flow-topography interaction problem, with emphasis on a range of parameters relevant to the large-scale motion of the atmosphere. We shall be able to expose certain important physical processes, some of which, though present in previous studies, never drew enough or any attention.

The model considered is based on approximating the horizontal momentum by the geostrophic momentum (the geostrophic momentum approximation) leaving everything else formally unchanged. This idea which is due to Eliassen (1948) is a natural extension to three dimensions of Merkine's two-dimensional work (1975).

The problem is formulated in Section 2 for an inviscid, steady uniform flow directed toward an isolated topographic feature on an f-plane. The flow is bounded above by a rigid lid but extends indefinitely horizontally. The Boussinesq approximation is made with a constant Brunt-Väisälä frequency. Section 3 presents numerical results describing flow response to different topographies for various values of stratification and upstream velocity. Special attention is given to those aspects of the flow field which are shown

to be independent of the upstream velocity. The problem of blocking is discussed in connection with the initial value and closed streamlines problems. Section 4 summarizes the results. Appendix A describes the numerical scheme. Appendix B discusses the range of validity of the geostrophic momentum approximation and compares it with the quasi-geostrophic approximation.

2. Formulation of the model

We start with the hydrostatic-Boussinesq form of the equations of motion describing steady inviscid flow past an isolated mountain on an f-plane:

$$\frac{Du'}{Dt'}=-\frac{1}{\rho_m}\frac{\partial p'}{\partial x'}+fv', \tag{2.1}$$

$$\frac{Dv'}{Dt'}=-\frac{1}{\rho_m}\frac{\partial p'}{\partial y'}-fu', \tag{2.2}$$

$$0=-\frac{1}{\rho_m}\frac{\partial p'}{\partial z'}+\frac{g}{\theta_m}\theta', \tag{2.3}$$

$$\frac{\partial u'}{\partial x'}+\frac{\partial v'}{\partial y'}+\frac{\partial w'}{\partial z'}=0, \tag{2.4}$$

$$\frac{D\theta'}{Dt'}+\frac{\theta_m}{g}N^2w'=0, \tag{2.5}$$

where

$$\frac{D}{Dt'}=u'\frac{\partial}{\partial x'}+v'\frac{\partial}{\partial y'}+w'\frac{\partial}{\partial z'} \tag{2.6}$$

is the time derivative following a fluid particle and primes denote dimensional variables; p' and θ' are the deviation of pressure and potential temperature from the basic hydrostatic state; the subscript m denotes representative values of the basic state and N is a constant Brunt-Väisälä frequency; and $\mathbf{g}$ is the effective gravitational acceleration parallel to $\frac{1}{2}\mathbf{f}$, the rotation vector, where f is a constant Coriolis parameter. [The viscous boundary layers can be neglected provided $\mathrm{Ro}\gg\mathrm{E}^{\frac{1}{2}}$, where Ro and E are characteristics Rossby and Ekman numbers of the flow. For topography whose characteristic length is several hundreds of kilometers, $\mathrm{Ro}\approx 0.3$ is a conservative estimate. Even with ν, the vertical eddy viscosity coefficient, as large as 10 $\mathrm{m^2\ s^{-1}}$ (Holton, 1972), $\mathrm{E}(=\nu/fH^2)\approx 3\times 10^{-2}$. Thus, in atmospheric conditions this constraint is usually satisfied.] Fig. 1 describes schematically the geometry of the problem. H is the undisturbed depth of the system bounded above by a rigid lid, and h is the maximum height of the topography whose functional shape is given by $F(x'/L_x, y'/L_y)$ where L_x and L_y are topographic characteristic scales in the x and y directions, respectively. We treat an isolated topographic feature and place a coordinate system such that $F_{\max}=F(0,0)=1$.

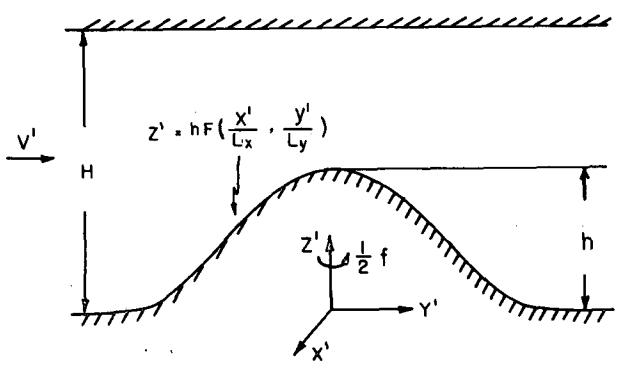

FIG. 1. Schematic of the geometric characteristics of the topography.

The flow is barotropic upstream and driven in the positive y direction. It is convenient to split the pressure field as follows:

$$\frac{1}{\rho_m}p'=fV_{-\infty}x'+\phi'(x',y',z'), \tag{2.7}$$

where ϕ' is the perturbation pressure field induced by the flow-topography interaction and $V_{-\infty}$ the upstream unperturbed velocity.

We now introduce the geostrophic momentum approximation according to which the momentum in the horizontal momentum equations is replaced by the geostrophic momentum, whereas the total time derivative is formally left unchanged. This approximation was originally introduced by Eliassen (1948), Fjortøft (1962) and recently by Hoskins (1975). It is considered to be more powerful than the quasi-geostrophic approximation and perhaps comparable but easier to handle than the balance equations (Charney, 1962). The approximation is the natural extension to three dimensions of the analysis of Robinson (1960), Jacobs (1964) and Merkine (1975) of two-dimensional flow over long topography.

Upon introducing the geostrophic momentum approximation into the horizontal momentum equations and making use of (2.7), Eqs. (2.1) and (2.2) are replaced by

$$\frac{Du_g'}{Dt'}=-fV_{-\infty}\frac{\partial\phi'}{\partial x'}+fv', \tag{2.8}$$

$$\frac{Dv_g'}{Dt'}=-\frac{\partial\phi'}{\partial y'}-fu', \tag{2.9}$$

respectively, where

$$(u_g',v_g')\equiv\left(-\frac{1}{f}\frac{\partial\phi'}{\partial y'},\frac{1}{f}\frac{\partial\phi'}{\partial x'}+V_{-\infty}\right). \tag{2.10}$$

The formal condition for the validity of the approximation is that

$$\frac{1}{f}\left(\left|\frac{D^2u'}{Dt'^2}\right|, \left|\frac{D^2v'}{Dt'^2}\right|\right) \ll f(|u'|, |v'|). \tag{2.11}$$

It is convenient at this stage to nondimensionalize the system. We restrict ourselves to mid-latitude atmospheric conditions with $f \approx 10^{-4}$ s^{-1}, $N \approx 10^{-2}$ s^{-1} and $H \approx 10^4$ m. It has been demonstrated by Merkine (1975) that the radius of deformation, defined as $L_R = NH/f$, is the proper horizontal length scale provided L_R is larger than the corresponding mountain scale. Implied in this condition is the requirement that the mountain be sufficiently wide for rotation to affect the dynamics of the flow. This condition is satisfied at least for the narrow cross section of the major continental mountain ridges of our planet. Consequently L_R is chosen as the appropriate horizontal length scale.

We shall demonstrate that the flow perturbations resulting from the mountain-flow interactions are to some extent independent of the undisturbed pressure gradient driving the flow toward the mountain. In the framework of an inviscid analysis that part of the response which is independent of the upstream velocity persists even as the upstream velocity tends to zero *provided it has alredy been established.* The vertical velocity is the only variable directly proportional to the upstream velocity. Consistent with these assertions, we introduce the following normalization:

$$\left.\begin{aligned} (x',y') &= L_R(x,y) \\ z' &= HZ \\ (u',v') &= L_R f(u,v) = NH(u,v) \\ w' &= fHV_0 w, \quad V_0 = V_{-\infty}/NH \\ \phi' &= f^2 L_R{}^2 \phi = (NH)^2 \phi \\ \theta' &= \frac{\theta_m}{g}\frac{f^2 L_R{}^2}{H}\theta = \frac{\theta_m}{g}N^2 H\theta \end{aligned}\right\} \tag{2.12}$$

The limit $V_0 \to 0$ implies no vertical velocity. It should be pointed out that all perturbation quantities are implicitly proportional to the height of the topography. Nevertheless, we have chosen not to explicitly exhibit this fact since we are dealing with finite topography. Consequently, the magnitude of the perturbation field as estimated in (2.12) is exaggerated by about a factor of 3 for the cases considered here.

Upon introducing (2.12) into the equation of motion the following system is obtained:

$$\begin{bmatrix} -\phi_{xy} & -\phi_{yy}-1 & -\phi_{yz} \\ \phi_{xx}+1 & \phi_{xy} & \phi_{xz} \\ \phi_{xz} & \phi_{yz} & \phi_{zz}+1 \end{bmatrix} \begin{bmatrix} u \\ v \\ w \end{bmatrix} = \begin{bmatrix} -V_0-\phi_x \\ -\phi_y \\ 0 \end{bmatrix} \tag{2.13}$$

$$\frac{\partial u}{\partial x}+\frac{\partial v}{\partial y}+\frac{\partial w}{\partial z}=0. \tag{2.14}$$

The first equation of (2.13) represents the x-momentum equation, the second equation represents the y-momentum equation, and the third equation represents the thermal energy equation. The condition for the validity of the approximation becomes

$$\left(\left|\frac{D^2u}{Dt^2}\right|, \left|\frac{D^2v}{Dt^2}\right|\right) \ll (|u|, |v|). \tag{2.15}$$

We can solve (2.13) for u, v and w to obtain

$$u = -\frac{1}{q}\left[\frac{\partial(\phi_z+z, \mathcal{H})}{\partial(y,z)} + V_0[\phi_{yz}\phi_{zx} - \phi_{xy}(\phi_{zz}+1)]\right], \tag{2.16a}$$

$$v = -\frac{1}{q}\left[\frac{\partial(\phi_z+z, \mathcal{H})}{\partial(z,x)} + V_0[(\phi_{xx}+1)(\phi_{zz}+1) - \phi_{zx}^2]\right], \tag{2.16b}$$

$$w = -\frac{1}{q}\left[\frac{\partial(\phi_z+z, \mathcal{H})}{\partial(x,y)} + V_0[\phi_{xy}\phi_{zx} - \phi_{yz}(\phi_{xx}+1)]\right], \tag{2.16c}$$

where

$$\mathcal{H} \equiv \tfrac{1}{2}(\phi_x{}^2+\phi_y{}^2+\phi_z{}^2)+\phi, \tag{2.17}$$

$$\begin{aligned} q \equiv\ & (\phi_{xx}+1)(\phi_{yy}+1)(\phi_{zz}+1) - \phi_{xy}^2(\phi_{zz}+1) \\ & - \phi_{yz}^2(\phi_{xx}+1) - \phi_{zx}^2(\phi_{yy}+1) \\ & + 2\phi_{xy}\phi_{yz}\phi_{zx}. \end{aligned} \tag{2.18}$$

$\mathcal{H}$ is that part of the particle's total energy which is independent of the upstream velocity. It is governed by

$$\frac{D}{Dt}(\mathcal{H} + \phi_x V_0 + \tfrac{1}{2}V_0 x) = 0. \tag{2.19}$$

The determinant q of the coefficient matrix of (2.13) is to be identified with a modified potential vorticity conserved following fluid particles. In other words,

$$\frac{Dq}{Dt} = 0 \tag{2.20}$$

as can easily be demonstrated by multiplying (2.16a, b, c) by q, applying the divergence operator, and utilizing the continuity equation (2.14). We can also

write q as

$$q=\boldsymbol{\zeta}_g\cdot(\nabla\phi+\mathbf{k}), \tag{2.21}$$

where

$$\boldsymbol{\zeta}_g=\left(-\phi_{xz}+\frac{\partial(\phi_x,\phi_y)}{\partial(y,z)},\ -\phi_{yz}+\frac{\partial(\phi_x,\phi_y)}{\partial(z,x)},\ 1+\phi_{xx}+\phi_{yy}+\frac{\partial(\phi_x,\phi_y)}{\partial(x,y)}\right) \tag{2.22}$$

is the modified vorticity defined only in terms of the geostrophic momentum. It is governed by the equation

$$\frac{D\boldsymbol{\zeta}_g}{Dt}=(\boldsymbol{\zeta}_g\cdot\nabla)\mathbf{u}-\mathbf{k}\times\nabla\phi. \tag{2.23}$$

Here $\mathbf{k}$ is a unit vector directed along the positive z-direction. It is important to point out that both the vorticity and the potential vorticity are independent of upstream velocity.

Our inviscid steady-state model explicitly assumes that all fluid particles have originated upstream and have carried with them their original potential vorticity and potential temperature. It implies that

$$q\equiv 1. \tag{2.24}$$

From conservation of potential temperature we have

$$\frac{D}{Dt}(\phi_z+z)=0\rightarrow\phi_z+z=Z_0, \tag{2.25}$$

where Z_0 is the upstream elevation or equivalently the potential temperature of a fluid particle. Eq. (2.25) permits us to write the top and bottom boundary conditions as

$$\phi_z=0 \text{ at } z=1, \tag{2.26}$$

$$\phi_z=\alpha F(S_x^{\frac{1}{2}}x, S_y^{\frac{1}{2}}y) \quad \text{at } z=\alpha F(S_x^{\frac{1}{2}}x, S_y^{\frac{1}{2}}y)=\alpha F(\xi,\eta), \tag{2.27}$$

where

$$\alpha=\frac{h}{H},\quad S_x^{\frac{1}{2}}=\frac{L_R}{L_x},\quad S_y^{\frac{1}{2}}=\frac{L_R}{L_y}.$$

S_x and S_y can be considered as the x and y Burger numbers of the flow, respectively.

The requirement that the perturbation pressure field ϕ decays away from the topography and that only the undisturbed geostrophic field exists at infinity leads to the boundary condition

$$(\phi_x,\phi_y)\rightarrow 0 \text{ as } (|x|,|y|)\rightarrow\infty. \tag{2.28}$$

It is important to point out that a strictly two-dimensional problem would lead to boundary conditions different than those of (2.28) (Merkine, 1975). It is one of the peculiarities of rotating systems that flow response to *long but finite* topography cannot be approximated by considering the response to an infinitely long topography.

The last few paragraphs indicate that the perturbation pressure field is determined by the elliptic boundary value problem (2.18), (2.24) and (2.26)–(2.28). The parameters of this sytem of equations appear only in the lower boundary condition (2.27). They affect the shape of the topography in such a way that an increase in stratification would always result in an apparent steeper topography.

It is a property of the model that the ϕ field and the isentropic surfaces $\phi_z+z=Z_0$ are determined independently of V_0, the upstream velocity. Once the pressure field is obtained the velocity field follows from (2.16). This important conclusion suggests that a quasi-static change in the upstream velocity would result only in a different streamline pattern on the fixed potential temperature surfaces.

Inspection of Eqs. (2.16) implies that the velocity field consists of two parts: one independent of and the other dependent on the upstream velocity. In order to isolate the first part V_0 should approach zero. The usual form of the inviscid top and bottom boundary conditions

$$w=0 \quad \text{at } z=1, \tag{2.29}$$

$$w=\frac{\alpha}{V_0}[S_x^{\frac{1}{2}}uF_\xi+S_y^{\frac{1}{2}}vF_\eta] \quad \text{at } z=\alpha F(\xi,\eta), \tag{2.30}$$

leads to the conclusion that as $V_0\rightarrow 0$ the flow at the ground must follow height contours with $w=0$ at the ground. This reasoning can be applied to any potential temperature surface. The obvious conclusion is that, in the absence of upstream velocity, $w=0$ identically. In this case fluid particles must follow closed trajectories along constant height contours of the potential temperature surfaces.

We have arrived at the very important result that the elliptic boundary value problem possesses a topographically bound vortex as a fundamental solution. This vortex is independent of the upstream velocity and its characteristics are determined solely by the state of the system, that is, stratification, rotation, and the nature of the topography. In the next section we analyze this vortex in order to gain better understanding of the flow response not associated with the upstream velocity. For an isolated mountain with a single peak the topographically bound vortex must fundamentally be anticyclonic since the potential temperature gradient is away from the mountain and the disturbance is expected to decay with height. Similarly a valley would generate a topographically bound cyclonic vortex. Experimentalists may find this discussion stimulating since by generating the topographically bound vortex with zero upstream velocity they can simulate and observe the stability charac-

teristics of a zonal flow which is sheared both horizontally and vertically.

When the upstream velocity is different from zero the flow pattern is some combination of a uniform velocity interacting with the ϕ field and a three-dimensional, anticyclonic, topographically-bound vortex. (For a quasi-geostrophically linearized system these two aspects of the flow field can be superimposed linearly and ϕ is governed by a three-dimensional Laplacian.) For a sufficiently strong upstream velocity the topographically bound vortex is being continuously replenished everywhere by new fluid particles arriving from infinity with their potential temperature and potential vorticity. In the absence of forcing the vortex becomes Lagrangian in nature and consists of the same fluid particles for all time. Such a vortex cannot sustain itself indefinitely in a real fluid and it is ultimately destroyed by turbulence through a spin-down process which may be enhanced by instabilities.

3. Results and discussion

In this section we present and discuss some solutions to the boundary value problem formulated in the previous section. We have considered an isolated mountain given in dimensional form by

$$z'=h\exp\left\{-\ln 2\left[\left(\frac{x'}{L_x}\right)^2+\left(\frac{y'}{L_y}\right)^2\right]\right\}, \qquad (3.1a)$$

and in nondimensional form by

$$z=\alpha\exp\{-\ln 2[S_x x^2+S_y y^2]\}, \qquad (3.1b)$$

where L_x and L_y define the height contour corresponding to 50% decrease in the mountain's elevation.

a. Range of physical parameters

Table 1 indicates the values of the nondimensional parameters and the corresponding physical variables for which numerical solutions were obtained. These values were chosen to be of meteorological interest. The method of solution and the accuracy of the results are discussed in Appendix A and Appendix B, respectively.

The solutions are arranged in three different groups, each corresponding to only one numerical solution of the boundary value problem governing the perturbation pressure field. Solutions IIIa and IIIb are grouped together because one can be obtained from the other by inverting x and y in the solution for ϕ. Comparison of II with either Ia or Ic enables us to study the effect of changing, respectively, the mountain scale or stratification, leaving everything else unchanged.

b. The potential temperature surfaces and the field of relative vorticity

The fundamental importance of the potential temperature surfaces was pointed out in Section 2. In this subsection we study the influence of stratification on these surfaces and draw certain conclusions with regard to the associated vorticity field.

The shape of the potential temperature surfaces for various cases of stratification is described in Fig. 2. The surfaces graphed are axially symmetric corresponding to a circular topography ($S_x=S_y=S$; $L_x=L_y=L$).

Fig. 2 indicates that the effect of an increase in stratification is to further perturb the free stream and to flatten all potential temperature surfaces, except those at the ground and top levels whose shape is fixed by the boundary conditions. This immediately implies that for strong stratification [$S\gtrsim O(1)$, which is of meteorological interest] the vertical gradient of potential temperature is maximum at the ground *only in the vicinity of the mountain.* A distances sufficiently far away from the mountain the gradient reaches its maximum at middle levels. Therefore, there is a region close to the ground in which the separation between potential temperature surfaces is larger than their separation at infinity. This point is also demonstrated in Fig. 3 which depicts the vertical displacement of potential temperature surfaces as a function of height at distances $r'=0$ and $r'=2L=L_R$ from the center of the mountain for the case $S=4$. This behavior is typical to all cases of strong stratification.

Conservation of potential vorticity implies that the vertical relative vorticity is negative/positive (anticyclonic/cyclonic) wherever the effect of the mountain is to decrease/increase the vertical separation of the

TABLE 1. Nondimensional parameters and corresponding physical variables for the various solutions.

Solution no.	α	S_x	S_y	V_0	f (10^{-4} s^{-1})	N (10^{-2} s^{-1})	L_x (10^6 m)	L_y (10^6 m)	H (10^4 m)	h (10^4 m)	$V_{-\infty}$ (10 m s^{-1})	Taylor column
Ia	0.3	1	1	0.1	1	1	1	1	1	0.3	1	yes
Ib	0.3	1	1	0.15	1	1	1	1	1	0.3	1.5	yes
Ic	0.3	1	1	0.3	1	1	1	1	1	0.3	3	no
II	0.3	4	4	0.15	1 1	1 2	$\frac{1}{2}$ 1	$\frac{1}{2}$ 1	1 1	0.3 0.3	1.5 3	no
IIIa	0.3	1	9	0.1	1	1	1	$\frac{1}{3}$	1	0.3	1	no
IIIb	0.3	9	1	0.1	1	1	$\frac{1}{3}$	1	1	0.3	1	yes

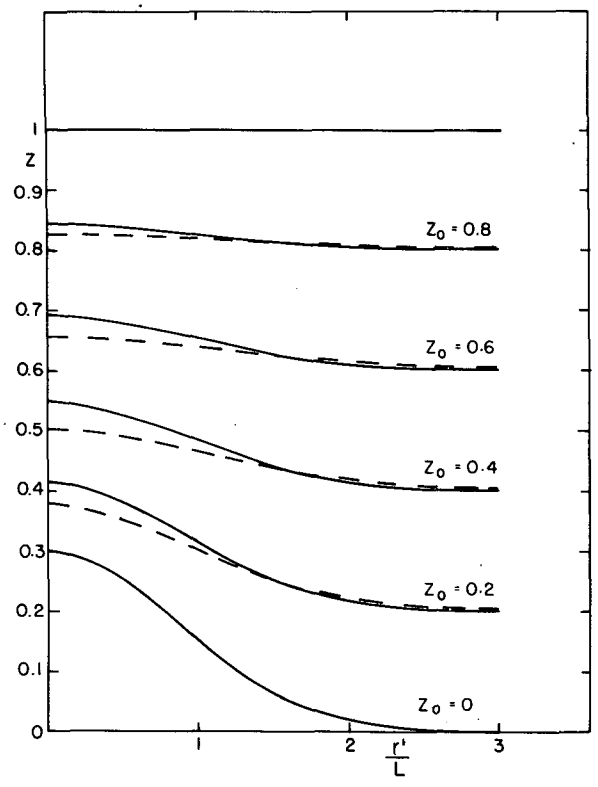

FIG. 2. Potential temperature surfaces: Z_0, upstream elevation; r'/L, radial distance. $S=1$ (full lines), $S=4$ (dashed lines).

potential temperature surfaces, with regard to their separation at infinity. Therefore, it follows from Figs. 2 and 3 that the field of relative vorticity is anticyclonic everywhere except for a shallow region near the ground far away from the mountain. This region possesses cyclonic vorticity Since the squashing of the potential temperature surfaces in the anticyclonic region is much stronger than their separation in the cyclonic region the vortex as a whole may be regarded as anticyclonic.

c. The bound vortex

In this subsection we analyze the bound vortex associated with the spatial configuration of the potential temperature surfaces. The topographically bound anticyclonic vortex is depicted in Fig. 4. The vortex is axially symmetric corresponding to a mountain with circular height contours. The azimuthal velocity is plotted both at the ground and top levels versus the radial distance measured in radii of deformation. The velocity is zero at the center, builds up almost linearly to a maximum located near the mountain's steepest slope, and then decays away with distance. This structure is similar to that of a vortex with finite core rotating with a constant angular velocity.

Fig. 4 demonstrates that the vortex is baroclinic in the vicinity of the mountain and barotropic in the far field. The barotropic character results from the fact that sufficiently far away from the mountain the ground level changes on a length scale which is larger than the radius of deformation. In other words, the local Burger number is less than unity. This implies that the local influence of stratification is secondary with the consequence of a height-independent structure.

It is characteristic to all strongly stratified fluids that a small change in stratification results in a large change in the vorticity field (compare Figs. 2 and 4).

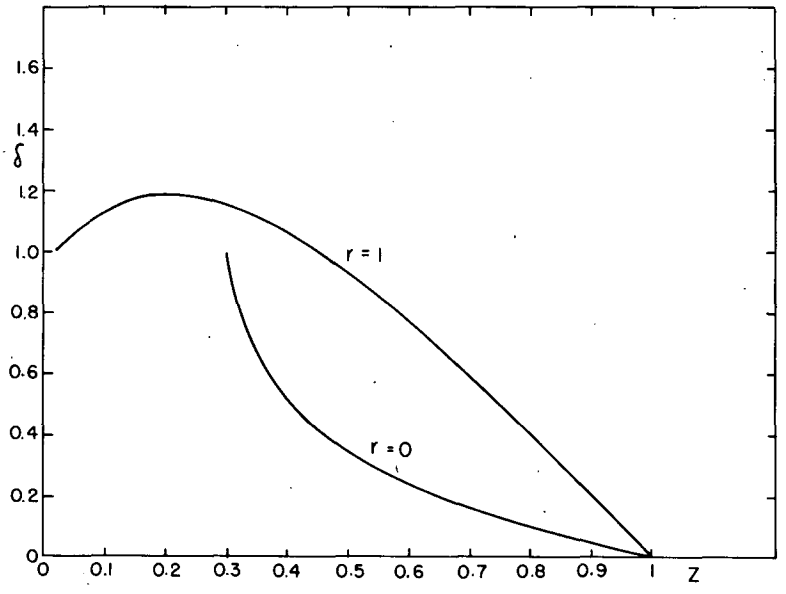

FIG. 3. Vertical distribution at two radial locations of the displacement of potential temperature surfaces δ normalized with respect to ground level value; $S=4$.

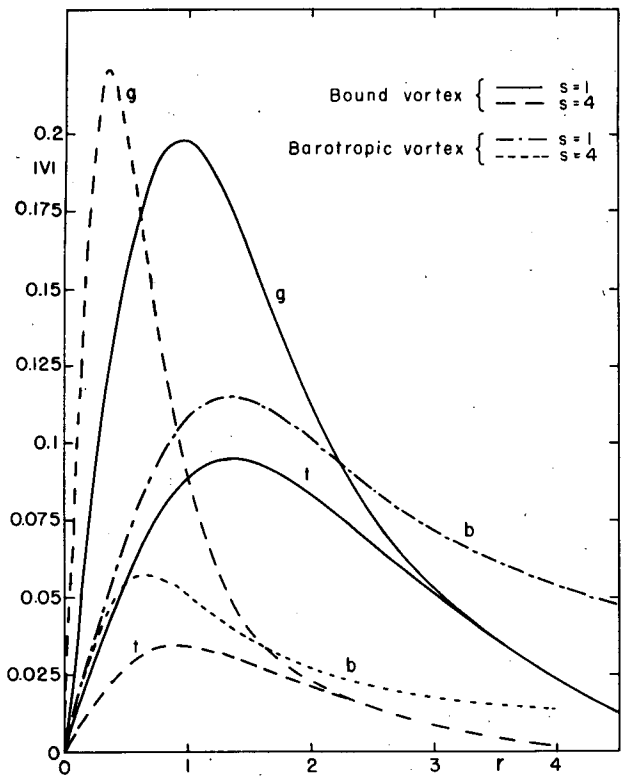

FIG. 4. Radial distribution of the velocity of the bound vortex at the ground (g) and top (t) levels. The barotropic (b) vortex, normalized according to (2.12), is also presented.

Therefore, Fig. 4 should provide us with a better picture of the role of stratification.

In order to understand the influence of the stratification parameter S it is convenient to regard a change in S as resulting either from a change in N or in L. A change in N implies that $S=4$ corresponds to an atmosphere which is twice as stratified and which has a radius of deformation which is twice as large as when $S=1$. It follows from Fig. 4 that an increase in stratification results in (i) approximately doubling the velocity of the vortex at the ground [Recall that the velocity is normalized by $L_R=NH$. This normalization is supported by Fig. 4 especially if the mountain's amplitude α is extracted.]; (ii) increasing both the vertical and horizontal shear; (iii) confining the vortex to lower elevations in the vicinity of the mountain; and (iv) pushing the disturbance farther away into the free stream. (The radius of deformation as well as the dimensional vortex velocity increase with N.)

If we interpret a change in S as resulting from a change in L leaving everything else unchanged then $S=4$ corresponds to a mountain which is twice as narrow as when $S=1$. Fig. 4 indicates that a narrow mountain induces stronger vertical and horizontal shear than a wider mountain but the maximum velocity at the ground is little affected by the mountain width. We also find that a narrow mountain exerts its influences well beyond the region it occupies. This fact poses a major challenge to general circulation models, since by not properly resolving the topography they may be losing more than a local flow response.

If we regard vortex shedding as a possible mechanism for mountain-induced cyclogenesis then an estimate of the strength of the shed vortex is warranted. A possible measure would be the circulation around it. Quasi-geostrophic analysis of homogeneous flow with rigid lid leads to the vorticity field

$$\zeta' = -f\frac{h}{H}\mathrm{F}\left(\frac{x'}{L_x}, \frac{y'}{L_y}\right). \tag{3.2}$$

The circulation around the bound vortex is given by

$$\Gamma^h_\infty = \int_{-\infty}^{\infty}\int_{-\infty}^{\infty} \zeta' dx' dy' = -\frac{f}{H}V_m = \mathrm{O}(\alpha f L^2), \tag{3.3}$$

where V_m is the volume of the mountain. If we use Kelvin's circulation theorem then the cyclonic vortex shed during the transient stage (Huppert and Bryan, 1975) must be of equal strength.

A simple integration of the vorticity field is not possible in a stratified fluid even in the framework of the quasi-geostrophic approximation. Nevertheless, Kelvin's theorem can be applied to a material ring moving on a potential temperature surface. We restrict ourselves to the rather special case in which the ground is a potential temperature surface for all time. For this case we can conclude that the magnitude of the circulation at the ground around the bound vortex and consequently around the shed vortex can be estimated using dimensional arguments as

$$\Gamma^s_\infty = \mathrm{O}(\alpha f L_R^2). \tag{3.4}$$

It follows from (3.3) and (3.4) that

$$\Gamma^s_\infty/\Gamma^h_\infty = \mathrm{O}(S) \quad \text{or} \quad \Gamma^s_\infty = \mathrm{O}\left(\frac{f}{H}V_m S\right). \tag{3.5}$$

This order of magnitude estimate suggests that a stratified shed vortex may be more violent at lower levels than a corresponding homogeneous vortex though its strength may diminish rapidly with height.

For the sake of completeness the velocity distribution of the quasi-geostrophic homogeneous bound vortex is also shown in Fig. 4. For the mountain considered this velocity is given dimensionally by

$$|v'| = \frac{1}{2\ln 2}\frac{h}{H}fL\frac{1}{(r'/L)}\left\{1-\exp\left[-\ln 2\left(\frac{r'}{L}\right)^2\right]\right\}. \tag{3.6}$$

The very slow decay of the homogeneous vortex is attributed to the effect of the rigid lid. A free surface would severely curtail the tail of such a vortex.

d. Taylor columns, the initial value problem, and the problem of blocking

The last column of Table 1 indicates whether or not closed streamlines are present in the numerical solutions. The formulation of the problem requires all fluid particles to have originated upstream with the consequence of establishing the ground as a constant potential temperature surface. Therefore, the fluid contained within such closed streamlines must have the same properties as the rest of the flow field. This restriction removes the non-uniqueness, usually associated with the presence of closed streamlines in an inviscid fluid, by requiring a *special* setup of the transient stage. During this stage the unperturbed pressure gradient must reach sufficient strength to establish the ground as a potential temperature surface. Once this has been established the unperturbed pressure gradient or equivalently the upstream velocity may approach any desired value. If the transient phase does not satisfy this constraint the steady state attained cannot be described by our model. An actual solution of the initial value problem is then required.

The last paragraph implies that the asymptotic value of the unperturbed pressure gradient is not sufficient for determining the final steady state. It is crucial to know, whenever closed streamlines are present, how this asymptotic value has been reached. Thus in the framework of an inviscid analysis we may have a multiplicity of steady-state solutions. This only underlines the importance of studying the initial value problem. It is of particular interest to examine the evolution of the system under a variety of setups in which the upstream velocity approaches monotonically and nonmonotonically the same final value.

It should be pointed out that any inviscid steady-state solution containing closed streamlines can resemble real fluid behavior (outside thin boundary layers) only if the transient time scale is short compared to the viscous time scale. This is usually the case in the atmosphere with the implication that steady-state *viscous* solutions have little practical interest. [The general problem of finding steady-state viscous solutions with closed streamlines is a very difficult one because the location of the outermost closed streamline and the state of the fluid within it are both unknown. The only recorded solution of this problem was obtained by Ingersoll (1969) for a flat top cylindrical mountain in a homogeneous fluid.]

The phenomenon of blocking is also related to the initial value problem. The question of determining in some quantitative way how much fluid goes around and how much goes over an obstacle in a rotating stratified system has not been answered yet. Huppert and Bryan (1975) attempted to answer this question using nondimensional arguments. They related the various nondimensional parameters of the problem to the vertical displacement of the heaviest fluid element touching at some horizontal location a plane tangent to the top of the mountain. Such a displacement, when normalized by the height of the mountain, ranges between zero and unity depending on the origin of the fluid particle. Their reasoning, which agrees well with their numerical results, seems to us to be satisfactory only when the unperturbed pressure gradient attains monotonically its final value. For if the ground is established as a potential temperature surface, as in our model, then regardless of the upstream velocity their criterion would indicate that the flow *always* goes over the topography yet closed streamlines may exist.

e. Trajectories of fluid particles for finite upstream velocities

The strongest horizontal velocities occur along the x-axis at ground level. At this cross section u and w are identically zero from symmetry consideration and the velocity field is an *algebraic* sum of the vortex velocity and a bell-shape velocity distribution which depends on the upstream velocity [see (2.16)]. Consequently, the anticyclonic vortex intensifies the velocity field on the left-hand side of the mountain (facing downstream) and diminishes it on the right-hand side. This effect is demonstrated in Fig. 5. Note that the jet-like region on the left-hand side of the mountain is much stronger than the vortex velocity at that region (Fig. 4).

Trajectories of fluid particles moving along ground and top levels are illustrated in Figs. 6–9. The shape of the trajectories resembles a typical orographic perturbation according to Queney (1973). The magnitude of the horizontal velocities exhibited in Fig. 5 together with the fact that we are considering mountains for which $S>O(1)$ justifies the neglect of the β-effect as can easily be demonstrated by a Rossby number expansion. These trajectories are also in qualitative agreement with the quasi-geostrophic trajectories of Ingersoll (1969), Hogg (1973) and Huppert (1975).

All trajectories possess cyclonic curvature on the wind and lee sides of the mountain and anticyclonic curvature over it. The cyclonic curvature vorticity at higher elevations must be accompanied by a stronger negative shear vorticity in order to generate a total vorticity field consistent with the conservation of potential vorticity (as discussed in subsection b).

Particle trajectories for solutian Ia are graphed in Fig. 6. Notable is the presence of a rather large Taylor column which is confined to lower levels. For this very wide mountain the upstream velocity required for the initiation of a Taylor column is in close agreement with the prediction of Huppert's quasi-geostrophic model (1975). (Fig. 6a contains more streamlines than Fig. 6b.)

The influence of stratification on the shape of the

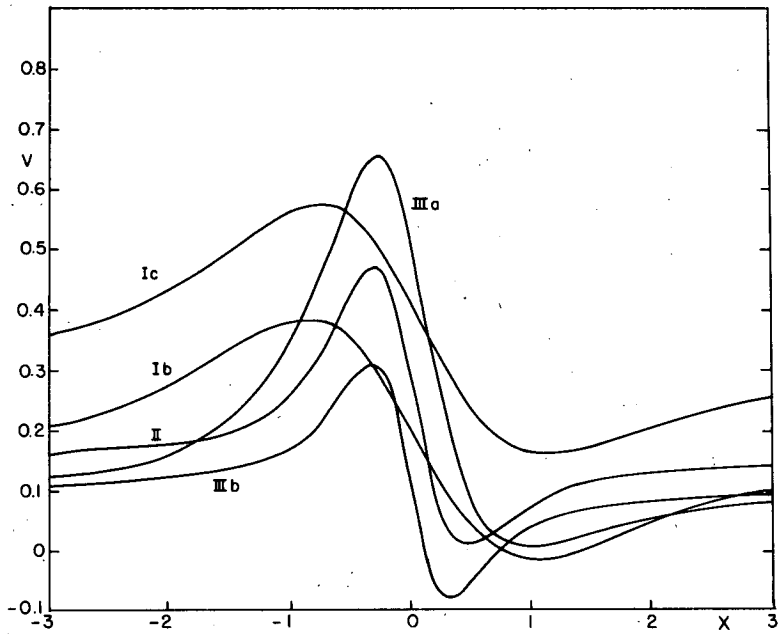

FIG. 5. Velocity distribution at ground level along the x-axis. Flow conditions are given in Table 1.

trajectories is illustrated in Fig. 7. Besides perturbing a larger fluid domain, an increase in stratification results in a greater tendency of fluid particles to go around the mountains. The latter effect can also be achieved by decreasing the upstream velocity leaving everything else unchanged. This is illustrated by comparing the full lines of Fig. 7 for which $V_0=0.3$ with the streamlines of Fig. 6 for which $V_0=0.1$.

So far our discussion has been concentrated on flow response to a circular topographic feature. From a meteorological point of view it is more appropriate to consider long ridges. Particle trajectories over a ridge whose axes have a 3:1 ratio are depicted in Figs. 8 and 9, where the small axis is either aligned with or perpendicular to the free stream (solutions IIIa and IIIb, respectively).

The mountain is more of an obstacle in the first case than in the second. Thus, it is surprising, at first sight, to find a Taylor column present in the second case but not in the first. The explanation of this behavior lies in the nature of the perturbation pressure field, which is the same for the two cases. This pressure field is quasi-two-dimensional along the long axis of the topography. When this axis is aligned with the free stream the perturbation pressure field has more time to impart momentum and to decelerate fluid particles moving on the right-hand side of the mountain (facing downstream) than when it is perpendicular to the free stream. Therefore, Taylor columns are more likely to appear when a mountain ridge is aligned with the free stream than otherwise. Taking into account the range of parameters as well as the shape and orientation of our continental mountain ridges, we may conclude that there is a slim likelihood for observing Taylor columns in the atmosphere. The situation may be different for the ocean as Taylor columns may have already been observed there (Hogg, 1973).

Finally, we should comment that the discussion of Figs. 8 and 9 suggests that whenever a flow field is approximately two-dimensional the rate of change of momentum perpendicular to the ignorable coordinate can be neglected in the momentum equations. Such a situation exists, for instance, in Charney's (1955) treatment of the Gulf Stream as an inertial boundary layer, in frontal structure (Hoskins and Bretherton, 1972), and in flow over a long ridge (Merkine, 1975).

4. Summary

We have attempted in this work to critically analyze inviscid steady flow over an isolated topographic feature in a stratified rotating atmosphere. Our model is based on approximating the horizontal momentum by the geostrophic momentum. This approach is considered comparable to solving the balance equations. The formulation leads to a boundary value problem governing the perturbation pressure field. The solution of this problem is shown to be an anticyclonic, topographically-bound vortex whose characteristics are independent of the upstream velocity but do depend on stratification, rotation, and the nature of the topography. The vortex is baroclinic in the vicinity of the mountain but barotropic in the far field. The

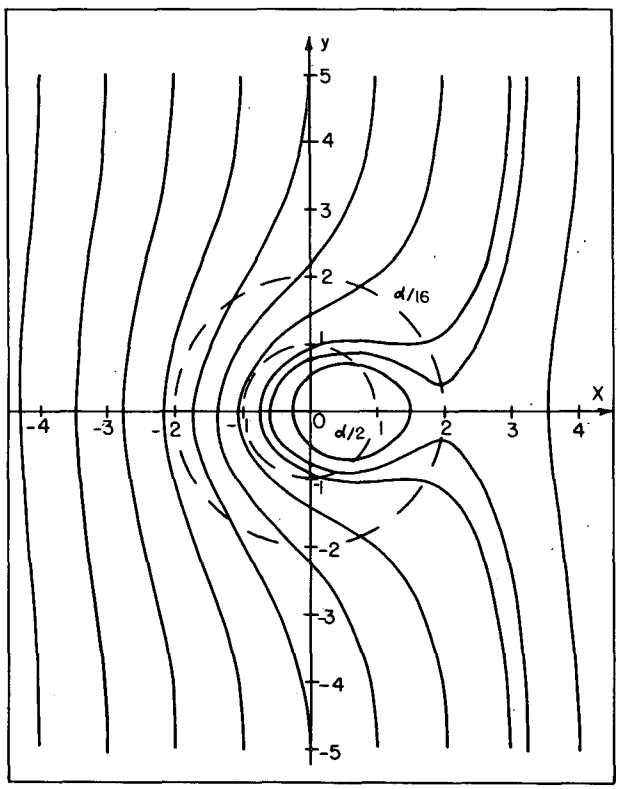

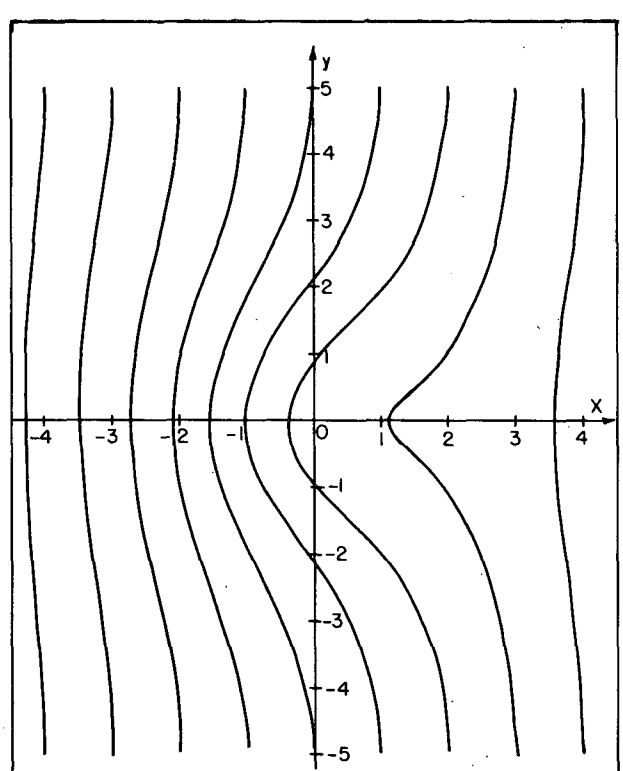

FIG 6. Particle trajectories derived from solution Ia at ground level (a) and top level (b). Topographic contours are indicated by dashed lines.

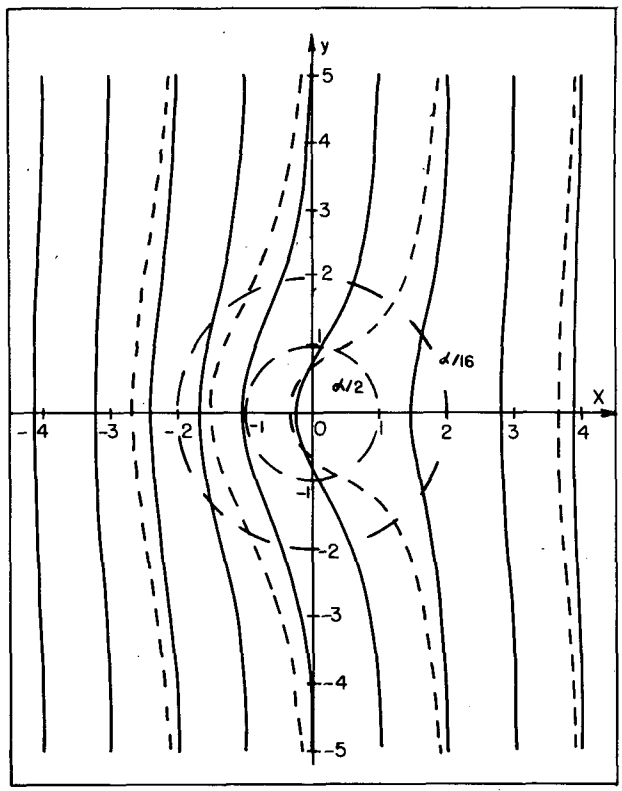

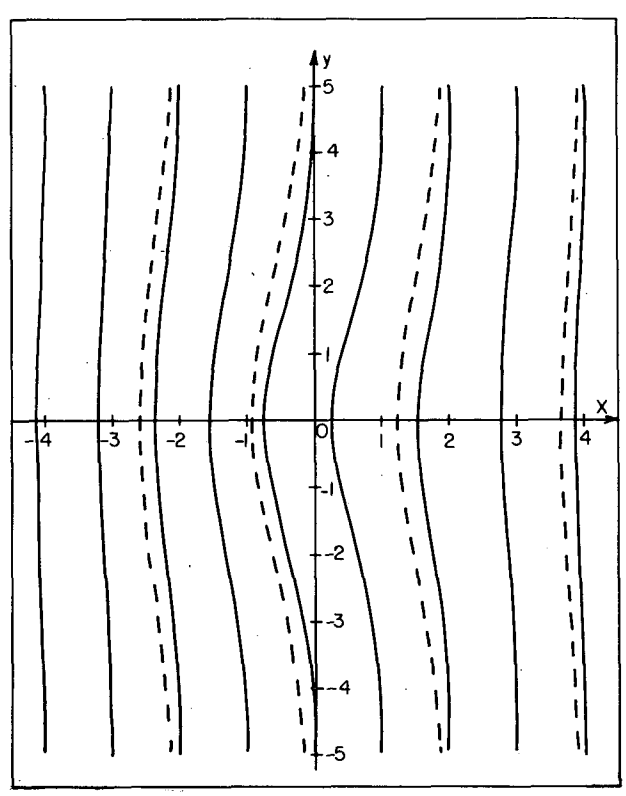

FIG. 7. Influence of an increase in stratification on particle trajectories: full lines, solution Ic; dashed lines, solution II. (a) Ground level, (b) top level. Topographic contours are indicated by dashed lines.

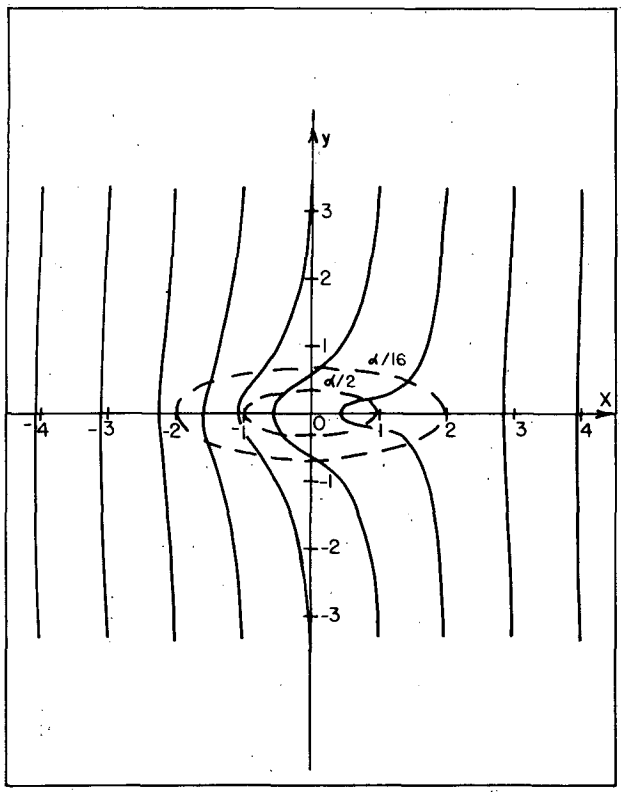

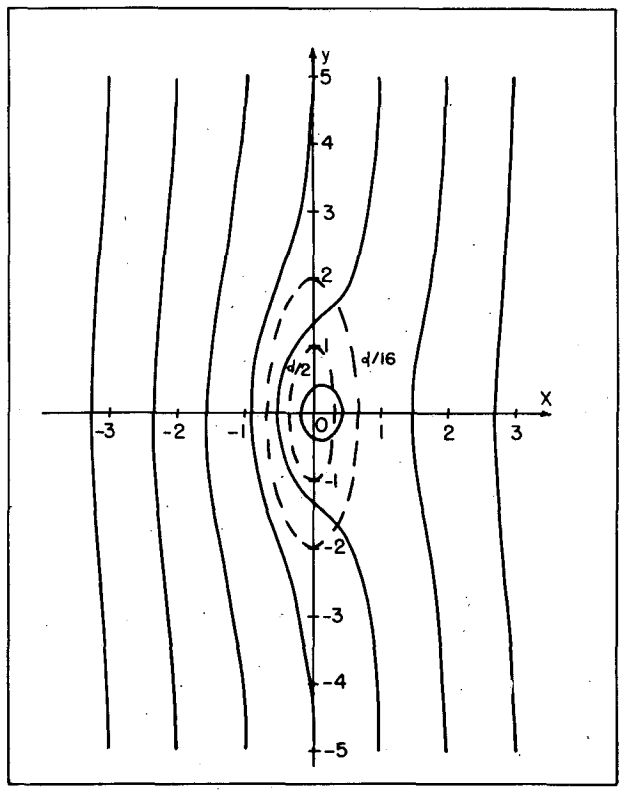

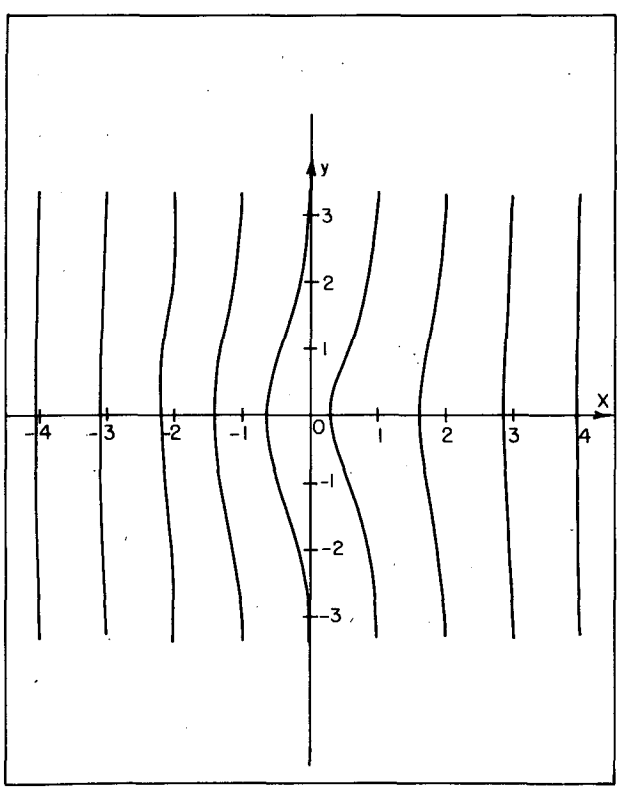

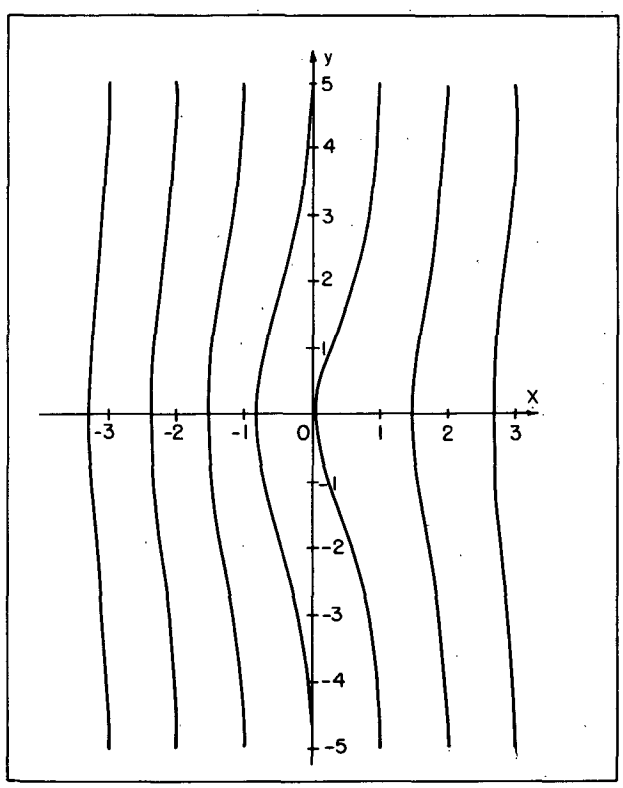

FIG. 8. Particle trajectories (solution IIIa) for a long ridge perpendicular to the free-stream direction. (a) Ground level, (b) top level. Topographic contours are indicated by dashed lines.

FIG. 9. Particle trajectories (solution IIIb) for a long ridge aligned with the free-stream direction. (a) Ground level, (b) top level. Topographic contours are indicated by dashed lines.

horizontal domain occupied by the disturbance scales on the radius of deformation. The implication with regard to atmospheric conditions is that even relatively narrow mountains can exert their influences over large distances. Intimately associated with the bound vortex are the potential temperature surfaces which are also independent of the upstream velocity. The total velocity field depends on the relative strength of the upstream velocity and the bound vortex. Flow tends to go around the mountain whenever stratification increases or the upstream velocity decreases. Nevertheless, it is argued that the problem of blocking and the question of uniqueness associated with closed streamlines can be answered properly only in the framework of the initial value problem. Currently we are attempting to answer these questions by modifying our model to include time-dependent solutions. The influence of upstream shear and the question of topographically induced baroclinic instabilities are problems we also hope to answer in the future.

Acknowledgments. We are grateful to Prof. Jule G. Charney for stimulating our interest in the problem of flow over mountains.

This research has been supported by the National Science Foundation under Grant NSF OCD 71-00333. The computations were performed at the National Aeronautics and Space Administration Goddard Institute for Space Studies in New York (NASA Grant NG R22-009-727).

APPENDIX A

Numerical Method of Solution

The equation of conservation of potential vorticity [(2.18) and (2.24)] can be written as

$$\nabla^2\phi = C(\phi), \tag{A1}$$

where

$$\begin{aligned} C(\phi) = (4/3)\{-1+[1+\tfrac{3}{2}[(\phi_{xx}-\phi_{yy}-\phi_{zz})^2/8 \\ +(\phi_{xx}+\phi_{yy}-\phi_{zz})^2/8+(\phi_{xx}-\phi_{yy}+\phi_{zz})^2/8 \\ +\phi_{xy}^2+\phi_{yz}^2+\phi_{zx}^2+\phi_{xy}\phi_{zz}+\phi_{yz}\phi_{xx}+\phi_{zx}^2\phi_{yy} \\ -\phi_{xx}\phi_{yy}\phi_{zz}-2\phi_{xy}\phi_{yz}\phi_{zx}]]^{\frac{1}{2}}\}, \end{aligned} \tag{A2}$$

$$\nabla^2\phi = \phi_{xx}+\phi_{yy}+\phi_{zz}. \tag{A3}$$

From Eq. (A1), the boundary conditions (2.26)–(2.28), and the shape of the topography (3.1), we conclude that ϕ is an even function in both x and y. Therefore, (A1) can be solved in the restricted domain $x\leqslant 0$, $y\leqslant 0$, $\alpha F(S_x^{\frac{1}{2}}x, S_y^{\frac{1}{2}}y)\leqslant z\leqslant 1$, subject to the boundary conditions

$$\left.\begin{aligned} &\phi_z=0 \quad \text{at } z=1 \\ &\phi_z+z=0 \quad \text{at } z=\alpha f(x,y),\ f(x,y)=F(S_x^{\frac{1}{2}}x, S_y^{\frac{1}{2}}y) \\ &\phi_x=0 \quad \text{at } x\to-\infty,\ x=0 \\ &\phi_y=0 \quad \text{at } y\to-\infty,\ y=0 \end{aligned}\right\}. \tag{A4}$$

We used a modified version of the σ-system of coordinates (Phillips, 1957) in order to make the ground and the top coordinate surfaces:

$$\sigma(x,y,z)=\frac{z-1}{1-\alpha f(x,y)}. \tag{A5}$$

The system (A1)–(A4) is solved in x,y,σ coordinates using the relationships

$$\left.\begin{aligned} [\phi_y]_{x,z} &= [\phi_y]_{x,\sigma}+\sigma_y\phi_\sigma \\ [\phi_{yy}]_{x,z} &= [\phi_{yy}]_{x,\sigma}+2\sigma_y[\phi_{y\sigma}]_{x,\sigma}+\sigma_{yy}\phi_\sigma+\sigma_y^2\phi_{\sigma\sigma} \\ \phi_z &= \sigma_z\phi_\sigma \\ \phi_{zz} &= \sigma_z^2\phi_{\sigma\sigma} \end{aligned}\right\},$$

and similar equations for the x- and cross-derivatives. Here the subscripts outside brackets indicate the variables held constant during the y-differentiation.

We solved (A1) with finite differences, using a uniform grid and 20 intervals in x, y and σ. Numerical tests indicated that an accurate solution was obtained when the boundary conditions at infinity were applied at $y=-5$ for $S_y=1$, $y=-4$ for $S_y=4$ and $y=-10/3$ for $S_y=9$, and similarly for x.

The method of solution was as follows: Given a guess ϕ^ν for ϕ, we computed $C(\phi^\nu)$ from (A2). Then we applied just one iteration of a relaxation scheme corresponding to

$$\nabla^2\phi = C(\phi^\nu), \tag{A6}$$

starting from ϕ^ν. The single relaxation iteration produced an improved approximation $\phi^{\nu+1}$, and the cycle was then repeated. It was found in previous two-dimensional computations that the procedure in which (A6) was solved completely, i.e., in which

$$\nabla^2\phi^{\nu+1} = C(\phi^\nu) \tag{A7}$$

was solved by relaxation, was unstable.

APPENDIX B

On the Accuracy of the Geostrophic Momentum Approximation

A discussion of the accuracy of the geostrophic momentum approximation is best started by considering the solution of the boundary value problem, i.e., the topographically-bound vortex. For simplicity we restrict ourselves to axially-symmetric mountains. For such a configuration the gradient wind relation

$$\frac{v^2}{r}+fv=\phi_r \tag{B1}$$

determines the exact relation between the pressure field and the velocity field provided the flow is steady. In (B1) v is the dimensional azimuthal velocity, ϕ the dimensional pressure, and r the local radius of curvature. The geostrophic momentum approximation to

(B1) is

$$\frac{v^a\phi_r}{fr}+fv^a=\phi_r \quad \text{or} \quad v^a=\frac{rf\phi_r}{f\phi_r+rf} \tag{B2}$$

[see also Hoskins (1975) and Fjortoft (1962)]. The superscript a indicates that (B2) provides only an approximated value to the velocity, where we have assumed that the pressure field is known exactly. We write

$$v^a=v(1-\epsilon), \tag{B3}$$

where ϵ is the error of the approximation, then substitute (B1) and (B3) into (B2) to obtain

$$\epsilon=\frac{\mathrm{Ro}^2}{1+\mathrm{Ro}+\mathrm{Ro}^2}, \quad \mathrm{Ro}\equiv\frac{v}{rf}, \tag{B4}$$

where Ro is the local Rossby number. A similar approach applied to the quasi-geostrophic system gives

$$\epsilon=-\mathrm{Ro}. \tag{B5}$$

We can conclude that the geostrophic momentum approximation is in this case one order of magnitude better than the quasi-geostrophic approximation. Furthermore, it always underestimates the velocity field though the representation is better for cyclonic regions than for anticyclonic regions. The quasi-geostrophic approximation, on the other hand, is seen to overestimate the velocity field in cyclonic regions and to underestimate it in anticyclonic regions.

In Table B1 we present the vortex velocity and the second total time derivative after about 3700 iterations corresponding to the case of $\alpha=0.3$, $S_x=S_y=4$ at $x=0$ and at ground level. The axial symmetry of the problem implies that u can be replaced by the azimuthal velocity and y by the radial distance; v would then represent the radial velocity which is identically zero. The neglected terms are seen to be small near the peak of the mountain where the vortex velocity is small or for distances larger than $y\approx0.5$ for which the curvature is no longer large [see also (B4)]. There is a small domain in which the neglected terms can no longer be considered as small. However, this is a shallow region and the accuracy of the approximation greatly improves with height. The reason for the *local* breakdown of the model is that in the shallow region the potential temperature surfaces are tightly packed together.

TABLE B1. Velocities and second total time derivatives corresponding to the case $S_x=S_y=4$ with $V_0=0$.

y	u	$\frac{D^2u}{Dt^2}$	v	$\frac{D^2v}{Dt^2}$
0	0	0	0	0
0.2	0.182	−0.117	0	0
0.4	0.219	−0.059	0	0
0.6	0.178	−0.015	0	0
0.8	0.130	−0.004	0	0
1.0	0.090	−0.001	0	0

TABLE B2. Numerical value of the individual terms in Eq. (A1) and of the geostrophic relative vorticity corresponding to the case $S_x=S_y=4$.

y	ϕ_{xx}	ϕ_{yy}	ϕ_{xz}	$\nabla^2\phi$	$C(\phi)$	ζ_g^z
0.0	−0.504	−0.504	3.161	2.153	2.144	−0.754
0.2	−0.464	−0.105	2.032	1.463	1.452	−0.520
0.4	−0.355	0.197	0.753	0.595	0.586	−0.228
0.6	−0.233	0.237	0.207	0.211	0.204	−0.051
0.8	−0.139	0.205	0.012	0.078	0.072	0.037
1.0	−0.081	0.151	−0.040	0.031	0.025	0.059
1.2	−0.048	0.099	−0.038	0.013	0.008	0.047
1.4	−0.031	0.061	−0.023	0.008	0.003	0.029
1.6	−0.021	0.039	−0.012	0.006	0.001	0.017
1.8	−0.015	0.026	−0.006	0.005	0.000	0.011
2.0	−0.012	0.020	−0.003	0.005	0.000	0.008

Table B2 presents numerical values of several terms of (A1). The value of the geostrophic vertical relative vorticity $\zeta_g^z=\nabla^2\phi+J(\phi_x,\phi_y)$ is also presented and may be interpreted as a measure of the local Rossby number *corresponding to the bound vortex*. $\zeta_g^z=0.005$ at $y=-4$. This is a measure of the error introduced by truncating the infinite domain. Table B2 indicates that for the mountain considered the quasi-geostrophic approximation is not adequate over most of the domain since $\nabla^2\phi$ is comparable to the individual second derivative terms.

Table B3 is the same as Table B1 except that now $V_0=0.15$. This corresponds to an overall Rossby number of 0.3 since $(V_{-\infty}/fL)=V_0S^{\frac{1}{2}}$. In this case the velocity field is no longer axially symmetric and thus cannot be described by a gradient wind formula. This table shows that the x-momentum equation is better satisfied than the y-momentum equation and that the accuracy of the approximation is worse than when $V_0=0$. Again we have found that the geostrophic momentum approximation improves with height.

We have also obtained the quasi-geostrophic solution for the case under discussion, i.e., $S=4$, $\alpha=0.3$. The vertical distribution of θ for the two approxima-

TABLE B3. As in Table A2 but with $V_0=0.15$.

y	u	$\frac{D^2u}{Dt^2}$	v	$\frac{D^2v}{Dt^2}$
0	0.182	−0.429	0.310	−0.570
0.2	0.219	−0.092	0.244	0.067
0.4	0.178	0.006	0.170	0.192
0.6	0.130	0.007	0.139	0.078
0.8	0.090	0.006	0.131	0.028
1.0	0.063	0.005	0.132	0.010

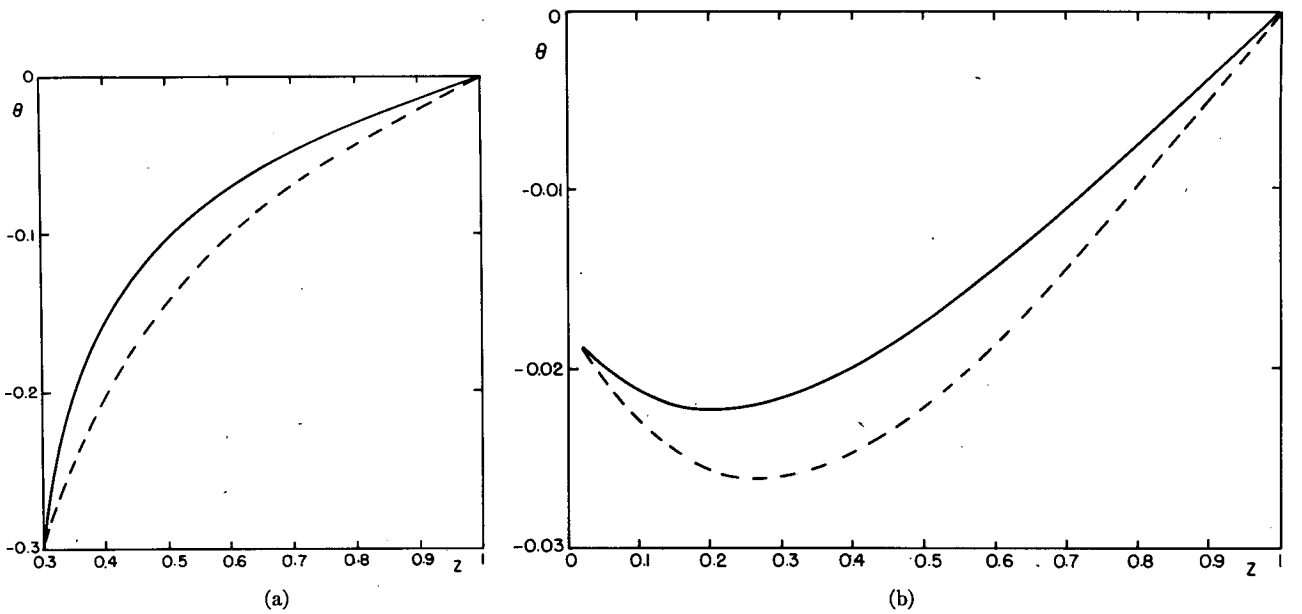

FIG. 10. Dynamic potential temperature θ vs height at (a) $r=0$ and (b) $r=1$: $S=4$, $\alpha=0.3$. Full lines, geostrophic momentum approximation; dashed lines, quasi-geostrophic approximation.

tions is depicted in Fig. 10. The difference between the two distributions is significant and most pronounced in middle levels, since the two approximations satisfy the same boundary conditions. Note that even at a distance of one radius of deformation from the center of the mountain the quasi-geostrophic approximation fails to properly describe the flow field. This is also demonstrated in Fig. 11 which compares the horizontal velocities of the two approximations along the x-axis and at ground level, $V_0=0.15$. Only

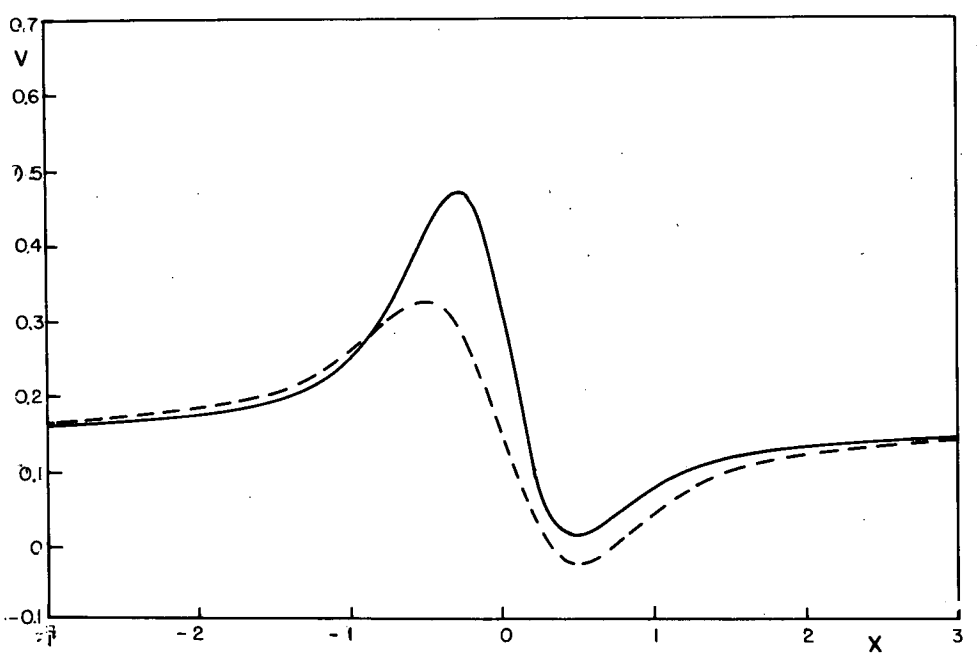

FIG. 11. Velocity distribution at ground level along the x-axis: $S=4$, $\alpha=0.3$, $V_0=0.15$. Full lines, geostrophic momentum approximation; dashed lines, quasi-geostrophic approximation.

beyond several radii of deformation from the center of the mountain are the two approximations seen to converge to the same solution.

It should be pointed out that the quasi-geostrophic approximation can be obtained from the geostrophic momentum approximation by neglecting the nonlinear terms in (2.16)–(2.18) and assuming that $V_0 \ll 1$. This renders V_0 as the geostrophic velocity at the top of the mountain. Note in Fig. 11 that the quasi-geostrophic approximation results in an antisymmetric distribution for the velocity whereas the geostrophic momentum approximation gives an asymmetric velocity distribution.

From the numerical results presented above and from other calculations performed we may say that for atmospheric conditions the model presented in this paper is adequate for describing flow response to finite topographic forcing for scales larger than 500 km and for $(V_{-\infty}/fL) \leqslant 0.3$. This is quite outside the range of the validity of the quasi-geostrophic approximation.

REFERENCES

Charney, J. G., 1955: The Gulf Stream as an inertial boundary layer. *National Academy of Sciences*, **41**, 731–740.

——, 1962: Integration of the primitive and balance equations. *Proc. Intern. Symp. Numerical Weather Prediction*, Meteor. Soc. Japan, Tokyo, 131–152.

Egger, J., 1972: Numerical experiments on the cyclogenesis in the Gulf of Genoa. *Beitr. Phys. Atmos.*, **45**, 320–346.

Eliassen, A., 1948: The quasi-static equations of motion. *Geofys. Publ.*, **17**, No. 3.

Fjortøft, R., 1962: On the integration of a system of geophysically balanced prognostic equations. *Proc. Intern. Symp. Numerical Weather Prediction*, Meteor. Soc. Japan, Tokyo 153–159.

Hogg, N. G., 1973: On the stratified Taylor column. *J. Fluid Mech.*, **58**, 517–537.

Holton, J. R., 1972: *An Introduction to Dynamic Meteorology*. Academic Press.

Hoskins, B. J., 1975: The geostrophic momentum equations and the semigeostrophic equations. *J. Atmos. Sci.*, **32**, 233–242.

——, and F. P. Bretherton, 1972: Atmospheric frontogenesis models: Mathematical formulation and solutions. *J. Atmos. Sci.*, **29**, 11–37.

Huppert, H. E., 1975: Some remarks on the initiation of inertial Taylor columns. *J. Fluid Mech.*, **67**, 397–412.

——, and K. Bryan, 1975: Topographically generated eddies (private communication).

Ingersoll, A. P. 1969: Inertial Taylor columns and Jupiter's Great Red Spot. *J. Atmos. Sci.*, **26**, 744–752.

Jacobs, S. J., 1964: On stratified flow over bottom topography. *J. Marine Res.*, **22**, 223–235.

McCartney, M. S., 1975: Inertial Taylor columns on a beta plane. *J. Fluid Mech.*, **68**, 71–95.

Manabe, S., and T. B. Terpstra, 1974: The effects of mountains on the general circulation of the atmosphere as identified by numerical experiments. *J. Atmos. Sci.*, **31**, 3–42.

Merkine, L., 1975: Steady finite-amplitude baroclinic flow over long topography in a rotating stratified atmosphere. *J. Atmos. Sci.*, **32**, 1881–1893.

Petterssen, S., 1956: *Weather Analysis and Forecasting*, Vol. 1, section 13.6. McGraw Hill.

Phillips, N. A., 1957: A coordinate system having some special advantages for numerical forecasting. *J. Meteor.*, **14**, 184–185.

Queney, P., 1973: *Dynamic Meteorology*, P. Morel, Ed. Reidel, 513–617.

Robinson, A. R., 1960: On two-dimensional inertial flow in rotating stratified fluid. *J. Fluid Mech.*, **9**, 321–332.